

## Controlled Design of Size-Tunable Monodisperse Nickel Nanoparticles

Sophie Carenco,<sup>†,‡</sup> Cédric Boissière,<sup>†</sup> Lionel Nicole,<sup>†</sup> Clément Sanchez,<sup>\*,†</sup> Pascal Le Floch,<sup>\*,‡</sup> and Nicolas Mézailles<sup>\*,‡</sup>

<sup>†</sup>UPMC Univ Paris 06 – Collège de France, Laboratoire de Chimie de la Matière Condensée de Paris, 11 place Marcelin Berthelot, 75231 Paris Cedex 05, France, and <sup>‡</sup>Laboratoire Hétéroéléments et Coordination, Ecole Polytechnique, CNRS, 91128 Palaiseau Cedex, France

Received July 6, 2009. Revised Manuscript Received December 18, 2009

We present here a complete study on a synthesis of nickel nanoparticles involving the reaction of  $[\text{Ni}(\text{acac})_2]$  with oleylamine (OA) and trioctylphosphine (TOP) reactants, whose simultaneous presence and relative amounts are paramount. The role of every reactant in the nucleation and growth of the nanoparticles has been delineated: OA is the reductant and thus controls the nucleation rate, meanwhile TOP provides a tunable surface stabilization through coordination on the Ni(0) surface. This result leads us to a design synthesis providing tailored monodispersed nanoparticles in a wide range (2–30 nm), which allows self-consistent studies of size-induced changes in catalytic and magnetic properties. Additionally, the growth mechanism is demonstrated to include an aggregation step which thus correlates with the polycrystalline feature of the nanoparticles obtained through this process. Moreover, the critical influence of the phosphine in this system was demonstrated a) for the outcome of the ripening mechanisms: defocusing effect and/or reshaping of the particles and b) for the surface properties: binding of the phosphine to the surface and its behavior toward oxidation was investigated by FTIR. Preliminary SQUID measurements show the impact of crystallites size on the magnetic properties.

### 1. Introduction

Size, shape, and surface state of metallic nanoparticles (NPs) are of paramount importance for a whole range of applications based on catalytic, optical, or magnetic properties.<sup>1,2</sup> Among all synthetic pathways, only a few have been understood in great detail after extensive studies, namely the Au(0) and Ag(0) systems.<sup>3</sup> The development of easy and well-defined syntheses giving access to a variety of size range, from clusters to bulk-like particles, becomes critical for precise studies of the size influence. Indeed, fine parameters such as the percentage of ligand coverage or a partial oxidation on the surface of the particles are not easily measured but strongly modulate catalytic activities or magnetic behavior. Among those parameters, the nature and abundance of surfactants, ligands, or stabilizers at the surface of the particles are critical for the outcome of the synthesis and consequently on the existence of any property of the particles.<sup>4–7</sup> Many models have been elaborated for the

nucleation and growth of the nanoparticles, highlighting the necessity to understand the role of every component in the synthesis.<sup>8–10</sup>

Monodispersed nickel nanoparticles display attractive properties in relation with their size. As a catalytic material, their activity has mainly been established in heterogeneous processes, where the surface of the metal is directly accessible.<sup>11</sup> An application is the homogeneous Suzuki cross-coupling recently reported by Hyeon et al. highlights the influence of the stabilizing ligand on the activity and selectivity of the catalyst.<sup>19</sup> Several synthetic approaches toward nickel nanoparticles have been developed, such as the polyol synthesis,<sup>12,13</sup> electrochemical reductions,<sup>14</sup> sol–gel

\*Corresponding author. Fax: (+33) 1 44 27 15 04. Tel: (+33) 1 44 27 15 02. E-mail: clement.sanchez@upmc.fr (C.S.). Fax: (+33) 1 69 33 44 49. Tel: (+33) 1 69 33 44 02. E-mail: pascal.lefloch@polytechnique.edu (P.L.F.). E-mail: nicolas.mezailles@polytechnique.edu (N.M.).

- (1) Hyeon, T. *Chem. Commun.* 2003, 927. Sun, S.; Murray, C. B.; Weller, D.; Folks, L.; Moser, A. *Science* 2000, 287, 1989.
- (2) Han, J.; Liu, Y.; Guo, R. *J. Am. Chem. Soc.* 2009, 131, 2060. Lee, I.; Delbecq, F.; Morales, R.; Albiter, M. A.; Zaera, F. *Nat. Mater.* 2009, 2, 132.
- (3) Grzelczak, M.; Perez-Juste, J.; Mulvaney, P.; Liz-Marzan, L. M. *Chem. Soc. Rev.* 2008, 37(9), 1783.
- (4) Yu, W. W.; Wang, Y. A.; Peng, X. *Chem. Mater.* 2003, 15, 4300.
- (5) Yin, Y.; Alivisatos, A. P. *Nature* 2005, 437, 664.
- (6) Garnweitner, G.; Niederberger, M. *J. Mater. Chem.* 2008, 18, 1171.
- (7) Zhiqiang, Y.; Klabunde, K. *J. Organomet. Chem.* 2009, 694, 1016.

- (8) Park, J.; Joo, J.; Kwon, S. G.; Jang, Y.; Hyeon, T. *Angew. Chem., Int. Ed.* 2007, 46, 4630. Casula, M. F.; Jun, Y. W.; Zaziski, D. J.; Chan, E. M.; Corrias, A.; Alivisatos, A. P. *J. Am. Chem. Soc.* 2006, 128, 1675.
- (9) Shevchenko, E. V.; Talapin, D. V.; Schnablegger, H.; Kornowski, A.; Festin, O.; Svedlindh, P.; Haase, M.; Weller, H. *J. Am. Chem. Soc.* 2003, 125, 9090. Cushing, B. L.; Kolesnichenko, V. L.; O'Connor, C. *J. Chem. Rev.* 2004, 104, 3893.
- (10) Polleux, J.; Pinna, N.; Antonietti, M.; Niederberger, M. *Adv. Mater.* 2004, 16(5), 436.
- (11) Xu, B. Q.; Wei, J. M.; Yu, Y. T.; Li, J. L.; Zhu, Q. M. *Top. Catal.* 2003, 22, 77. Haag, S.; Burgard, M.; Ernst, B. *J. Catal.* 2007, 252, 190.
- (12) Murray, C. B.; Sun, S.; Doyle, H.; Betley, T. *MRS Bull.* 2001, 26, 985.
- (13) Hinotsu, T.; Jeyadevan, B.; Chinnasamy, C. N.; Shinoda, K.; Tohji, K. *J. Appl. Phys.* 2000, 95, 7477. Tzitzios, V.; Basina, G.; Gjoka, M.; Alexandrakis, V.; Georgakilas, V.; Niarchos, D.; Boukos, N.; Petridis, D. *Nanotechnology* 2006, 17, 3750.
- (14) Sun, Y. P.; Rollins, H. W.; Guduru, R. *Chem. Mater.* 1999, 11, 7. Chen, D. H.; Hsieh, C. H. *J. Mater. Chem.* 2002, 12, 2412. Jeon, Y. T.; Moon, J. Y.; Lee, G. H.; Park, J.; Chang, Y. *J. Phys. Chem. B* 2006, 110, 1187. Zach, M. P.; Penner, R. M. *Adv. Mater.* 2000, 12, 878.

technique,<sup>15</sup> microwave heating,<sup>16</sup> seeding techniques,<sup>17</sup> or reduction of an organometallic precursor,<sup>18–21</sup> each of them leading to a specific size range. In this last category, a Ni(II) precursor is reduced either at low temperature with a strong reductant such as sodium tetrahydridoborate<sup>22</sup> or at high temperature by a mixture containing amine and/or carboxylic acid.<sup>23</sup> In the first case, the reductant is clearly identified, but the nucleation is swift thus hard to control. In the second case, the synthesis goes through complex mechanisms due to the apparition of intermediates (such as *in situ* formation of carboxylate complexes and acid–base equilibrium), which makes a tailored synthesis hardly reachable. An additional approach consists of decomposing a Ni(0) precursor, such as bis(cyclooctadiene)nickel, in the presence of a ligand, which allows for a good shape control.<sup>24–26</sup> The sole drawback of this method is the high reactivity of the air-sensitive Ni(0) precursors. However, it appears that most of these synthetic methods cannot give access to monodisperse particles with a broad range of size without critically modifying the nature of the stabilizing ligand and the reducer: this renders it difficult to both the understanding of the synthesis and the direct comparison of the size influence on a particular property. Moreover, the ripening mechanisms have rarely been discussed even though they are relevant for the final properties of the particles.

Here, we present a systematic investigation of the synthesis of Ni(0) nanoparticles by the thermal reduction of a Ni(II) precursor, using a binary ligand system consisting of an amine (oleylamine, OA) and a phosphine (triocetylphosphine, TOP). Although similar synthesis was already described in literature, the specific contribution of OA and TOP on nucleation and growth of Ni NPs were scarcely investigated. Our main goal in this study is to precisely delineate the role of each component in the reaction mixture. This understanding allowed us to define

- (15) Chatterjee, A.; Chakravorty, D. *Appl. Phys. Lett.* **1992**, *60*, 138.
- Yang, J.; Feng, B.; Liu, Y.; Zhang, Y.; Yang, L.; Wang, Y.; Wei, M.; Lang, J.; Wang, D.; Liu, X. *Appl. Surf. Sci.* **2008**, *254*, 7155.
- (16) Parada, C.; Morán, E. *Chem. Mater.* **2006**, *18*, 2719.
- (17) Grzelczak, M.; Perez-Juste, J.; Rodriguez-Gonzalez, B.; Spasova, M.; Barsukov, I.; Farle, M.; Liz-Marzan, L. M. *Chem. Mater.* **2008**, *20*, 5399.
- (18) Wang, H.; Jiao, X.; Chen, D. *J. Phys. Chem. C* **2008**, *112*, 18793.
- Chen, Y.; Luo, X.; Yue, G. H.; Luo, X.; Peng, D. L. *Mater. Chem. Phys.* **2009**, *113*, 412.
- Green, M.; O'Brien, P. *Chem. Commun.* **2001**, 1912.
- (19) Park, J.; Kang, E.; Son, S.; Park, H.; Lee, M.; Kim, J.; Kim, K.; Noh, H.; Park, J.; Bae, C.; Park, J.; Hyeon, T. *Adv. Mater.* **2005**, *17*, 429.
- (20) Chen, Y.; Peng, D.; Lin, D.; Luo, X. *Nanotechnology* **2007**, *18*, 505703.
- Zhang, H. T.; Wu, G.; Chen, X. H.; Qiu, X. G. *Mater. Res. Bull.* **2006**, *41*, 495.
- Goto, Y.; Taniguchi, K.; Omata, T.; Otsuka-Yao-Matsuura, S.; Ohashi, N.; Ueda, S.; Yoshikawa, H.; Yamashita, Y.; Oohashi, H.; Kobayashi, K. *Chem. Mater.* **2008**, *20*, 4156.
- (21) Han, M.; Liu, Q.; He, J. H.; Song, Y.; Xu, Z.; Zhu, J. M. *Adv. Mater.* **2007**, *19*, 1096.
- (22) Hou, Y.; Gao, S. *J. Mater. Chem.* **2003**, *13*, 1510.
- (23) Han, M.; Liu, Q.; He, J.; Song, Y.; Xu, Z.; Zhu, J. *Adv. Mater.* **2007**, *19*, 1096.
- (24) Bradley, J.; Tesche, B.; Busser, W.; Maase, M.; Reetz, M. *J. Am. Chem. Soc.* **2000**, *122*, 4631.
- (25) Ely, T. O.; Amiens, C.; Chaudret, B. *Chem. Mater.* **1999**, *11*, 526.
- Cordente, N.; Respaut, M.; Senocq, F.; Casanove, M. J.; Amiens, C.; Chaudret, B. *Nano Lett.* **2001**, *1*, 565.
- (26) Carenco, S.; Resa, I.; Le Goff, X.; Le Floch, P.; Mézailles, N. *Chem. Commun.* **2008**, 2568.

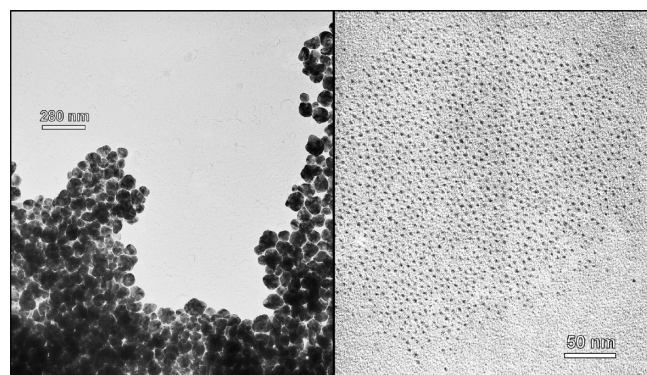


**Figure 1.** Left: nickel NPs synthesized with 10 equiv of OA (50–80 nm). Right: nickel NPs synthesized with 10 equiv of TOP (2 nm).

for the first time conditions for the rational synthesis of monodispersed Ni(0) particles with tailored sizes: ca. from 2 to 30 nm. In the present paper, we investigate the growth mechanism and evidence for the first time a crucial implication of aggregation in this process. Additionally, we were able to characterize two mechanisms of ripening affecting strongly the monodispersity and the morphology of the nanoparticles, for which we propose a rationalization based on the phosphine stoichiometry. As a first step toward application in the field of catalysis, the shell of ligands and its behavior at air contact is analyzed using IR spectroscopy. Additionally, we report preliminary magnetic characterization by SQUID, as an initial study supporting our designed pathway toward tailored monodispersed nickel nanoparticles.

## 2. Results and Discussion

In a typical synthesis,  $[Ni(acac)_2]$  was dissolved in a solution containing oleylamine ( $x$  equiv) and/or triocetylphosphine ( $y$  equiv). In order to make pertinent comparisons between the various experiments, the concentration of the Ni species had to be constant. This was achieved by the addition of appropriate amounts of 1-octadecene (ODE). The reaction mixture was then heated at  $220\text{ }^\circ\text{C}$  for 2 h, yielding a black solution of nanoparticles subsequently isolated by centrifugation and redispersed in hexanes.<sup>27</sup> The particles were systematically analyzed by XRD and TEM.

**2.1. Reduction of the Ni(II) Precursor by TOP.** In the first series of experiments, the effect of TOP was studied. Quite surprisingly, even at  $220\text{ }^\circ\text{C}$ , TOP was shown to be a poor reducing agent for the nickel complex  $[Ni(acac)_2]$ . Indeed, when the synthesis was conducted with 10 equiv of TOP (without oleylamine and without ODE), the complete reduction was far from being achieved within 2 h, as attested by the green-black color of the mixture (presence of starting  $[Ni(acac)_2]$ ). Only about 30% of the expected amount of nanoparticles was recovered upon precipitation. Nevertheless, the isolated particles were readily dispersed in nonpolar solvents such as hexanes. The TEM analysis (Figure 1, right-hand side) of these

(27) Note that it is well-known in the literature that the TOP ligand does not decompose at this temperature to form nickel phosphide particles but above  $330\text{ }^\circ\text{C}$ .

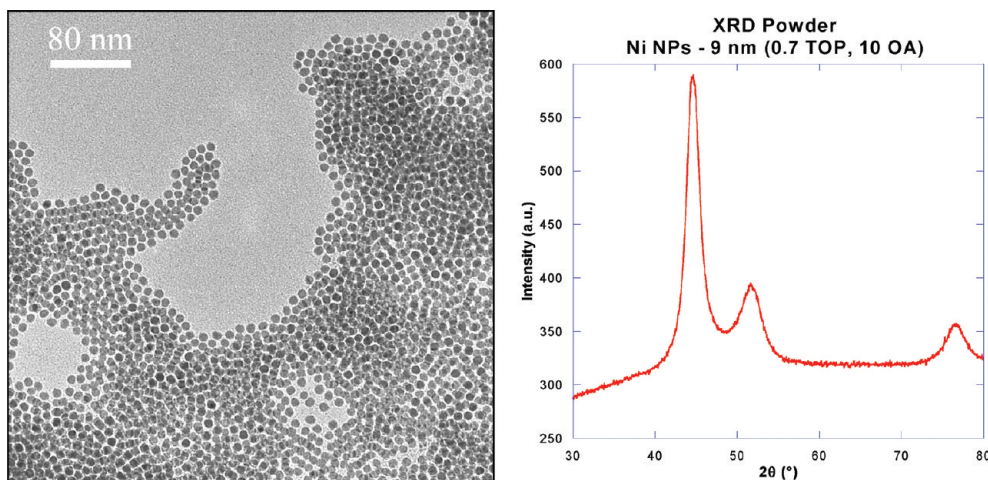
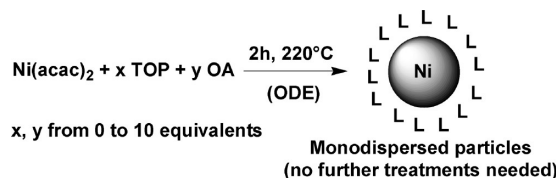


**Figure 2.** Nickel NPs synthesized with 10 OA and 0.8 TOP (9 nm,  $\sigma < 6.6\%$ ). XRD powder analysis on 9 nm nickel nanoparticles.

**Scheme 1. Synthetic Procedure (L = TOP and/or OA)**



particles revealed the formation of very small nanoparticles (2 nm,  $\sigma \approx 15\%$ ).<sup>28</sup>

Obviously, under these conditions, only a few nuclei are formed, and the presence of large amounts of TOP, an efficient ligand for Ni(0) species, prevents their growth, resulting in the formation of small nanoparticles.

**2.2. Reduction of the Ni(II) Precursor by OA.** On the contrary, the reduction was found to proceed very rapidly in the presence of 10 equiv of OA without phosphine. Once the temperature reached 220 °C, the solution turned completely black within less than 5 min. The reaction was stopped after 10 min, and the particles were all aggregated on the stir bar. They were readily redispersed in THF or hexanes upon sonication. TEM pictures (Figure 1, left-hand side) revealed the formation of polydisperse nanoparticles in the range of 50 to 80 nm, crystallized in the fcc structure (see ESI), consistent with results reported by Zhang et al., Chen et al., and Goto et al.<sup>20</sup> Under the reaction conditions, a fast reduction of the Ni(II) precursor occurred leading to an important concentration of Ni(0) species which are not efficiently stabilized by the ligands present in solution. In particular, OA is found to be a very poor ligand for Ni(0) nanoparticles, this point being extensively discussed in paragraph 2.8 (surface characterization by FTIR spectroscopy). This results in a fast aggregation process leading to polydisperse nanoparticles.

(28) The standard deviation  $\sigma$  in nanometre is calculated on a sample containing at least 100 nanoparticles and using the formula  $\sigma = (\bar{x} - \bar{\bar{x}})$  where  $\bar{x}$  is the mean of  $x$  value.  $\sigma$  in percent is obtained by reporting  $\sigma$  in nanometer to the mean size of the particles. The standard deviation is given as a maximum value because it has been observed that DigitalMicrograph introduces a significant incertitude (around 2%–5%) when it extracts binary data from the picture (creation of a border between the particle and the outside).

**Table 1. TEM Size of the Particles, Size of the Crystallites, and Corresponding Composition of the Reaction Mixture**

entry	TEM diameter (nm)	Scherrer diameter (nm)	equiv TOP per Ni	equiv OA per Ni
1	50–80	20.0	0	10
2	32 ( $\sigma < 7.2\%$ )	4.8	0.8	3
3	9 ( $\sigma < 6.9\%$ )	5.1	0.8	10

Major results of these experiments are as follows: a) there is a large difference in the kinetics of reduction of the Ni(II) precursor by the amine and the phosphine and b) the amine and phosphine ligands possess very different stabilizing abilities, as expected from classical Ni(0) complex organometallic chemistry. From these two studies, one could therefore reasonably assume that a) the amount of amine would influence the rate of nucleation and b) the phosphine would stabilize efficiently the growing particles. This would be an ideal situation for the synthesis of not only monodispersed but also size controlled particles. Experiments were thus carried out with various quantities of the two ligands to confirm these hypotheses.

**2.3. Synthesis of Monodispersed Ni Nanoparticles with 10 OA and  $x$  TOP.** The reaction was conducted with 10 equiv of OA as the reducing agent in order to favor a fast reduction, a prerequisite for the synthesis of monodispersed particles according to the accepted nucleation/growth formation mechanism of particles. When the reaction was first conducted with  $x = 0.8$  equiv of TOP as the main ligand, monodispersed particles of 9 nm were obtained (Figure 2), which confirmed the first hypothesis. The  $^{31}\text{P}$  NMR spectrum of the isolated nanoparticles redispersed in hexanes displayed a broad signal at  $-31.3$  ppm, consistent with an exchange of the phosphine between the solution and the particles surface, indicating that the particles are dynamically solvated (see ESI).<sup>5</sup> The particles also show a crystalline fcc structure (Figure 2), and the size of the crystalline domains (5.1 nm by the Scherrer formula, Table 1) is calculated to be smaller than the apparent size of the particles (9 nm).

Subtle changes in the stoichiometry of TOP appear to induce quite important changes in the resulting particles. In a mixture containing 10 equiv of OA and 0.1 equiv of

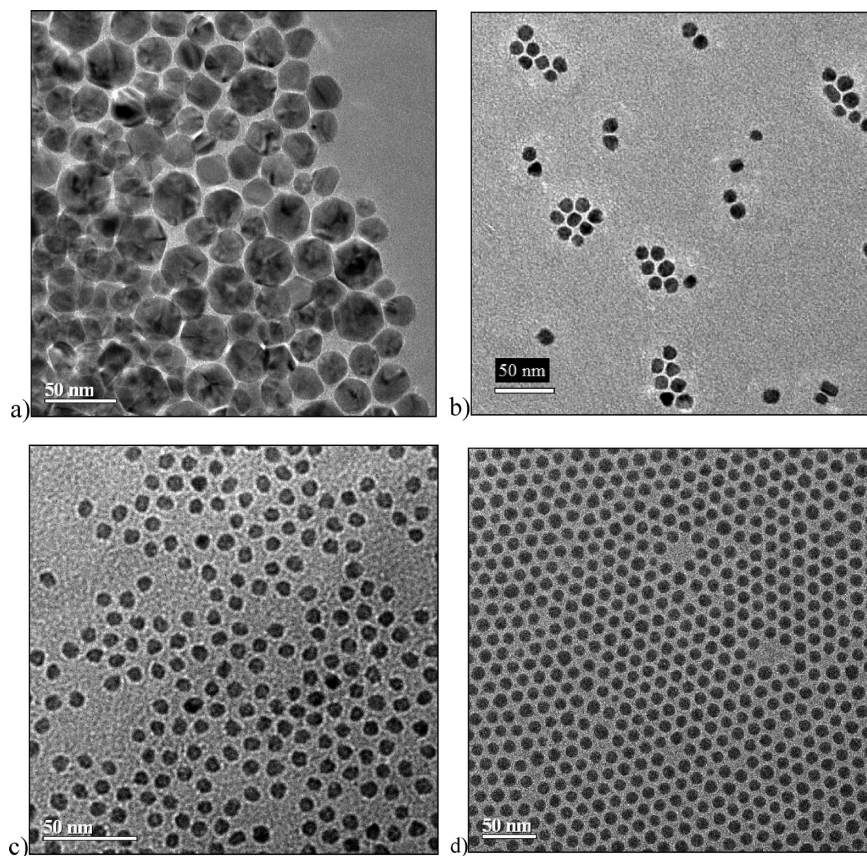


**Figure 3.** Nickel NPs synthesized with 10 OA and a) 0.1 TOP, b) 0.3 TOP, c) 0.5 TOP, and d) 5 TOP.

TOP, much smaller particles than without TOP are observed: average 25 nm with a broad size distribution. Increasing the amounts of TOP from 0.1 to 0.3 equiv resulted in a decrease of size of the particles to 13 nm, with a narrower distribution ( $\sigma < 10.1\%$ ). Facets are clearly observed on the particles. At 0.5 equiv the particles became monodisperse at 9 nm ( $\sigma < 7.9\%$ ), and in the 0.5 to 5 equiv range, the same size was observed for the particles (no facets,  $\sigma < 6.9\%$  for the synthesis with 5 equiv). These observations indicate that, with a large nucleation rate set by the OA amount, even minimal amounts of TOP stabilize the particles through coordination onto the surface and limit the aggregation of the nuclei (Figure 3). In the range of 0.5 to 5 equiv, the size of the particles remains the same. This indicates that the surface of the particles is probably saturated with phosphine, and the smaller size possible, in direct relation with the numbers of nuclei initially created, is achieved. However, a slight change in the shape was reproducibly observed: in the presence of larger amounts of TOP, the particles are devoid of facets and become completely spherical (Figure 3).

**2.4. Synthesis of Monodispersed Ni Nanoparticles with 0.8 TOP and  $y$  OA.** We have hypothesized above that the amount of OA correlates the reduction rate and therefore the quantity of nuclei produced. This would in turn lead to a control of the particle size. The effect of amount of OA was then studied. The results are quite straightforward. Reducing the amount of OA from 8 to 6, 4 then 2

equiv in the presence of 0.8 equiv of TOP, resulted in limiting the nucleation and promoting the growth of the particles, yielding monodisperse species of 23 nm ( $\sigma < 5.7\%$ ), 26 nm ( $\sigma < 5.1\%$ ), 28 nm ( $\sigma < 5.9\%$ ), and 32 nm ( $\sigma < 7.2\%$ ), respectively (Figure 4). The particles were found to be more faceted in these two latest cases. Note that in the first three cases, the reaction is complete (the metallic precursor is entirely consumed) as attested by the disappearing of the characteristic green color from  $[\text{Ni}(\text{acac})_2]$ , while using only 2 equiv of OA does not lead to a 100% yield, as attested by the green color of the supernatant after centrifugation. This suggests that more than 2 equiv of OA are necessary for the stoichiometric reduction of  $[\text{Ni}(\text{acac})_2]$  in these experimental conditions.

Overall, the studies presented above prove the role of OA (reducing agent at 220 °C) and TOP (stabilizing ligand) in the formation and stabilization of Ni nanoparticles. It remained to be proved that intermediate sizes could be obtained by adjusting the nucleation rate (quantity of amine) and the amount of phosphine. This was in fact readily done. For example, the reduction of the nickel precursor with 4 equiv of amine in the presence of 4 equiv of phosphine gave monodisperse particles of 15 nm (Figure 5). If the reduction is performed with 3 equiv of amine and 0.8 equiv of phosphine, monodisperse particles of 32 nm are obtained.

**2.5. Crystallographic Structure and Size of Crystalline Domain of Ni Nanoparticles.** The crystallographic structure of the nanoparticles was systematically investigated.

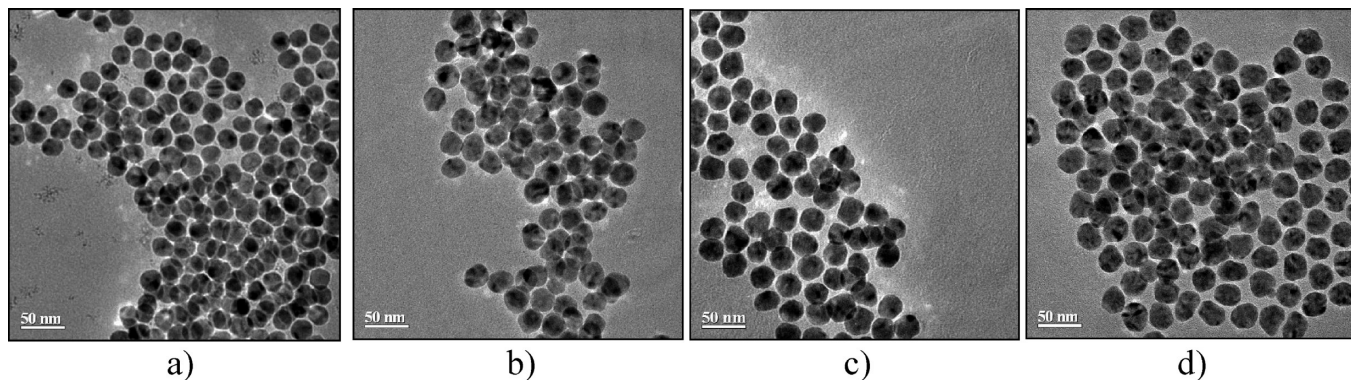


**Figure 4.** Nickel NPs synthesized with 0.8 TOP and a) 8 OA (23 nm), b) 6 OA (26 nm), c) 4 OA (28 nm), and d) 2 OA (32 nm).

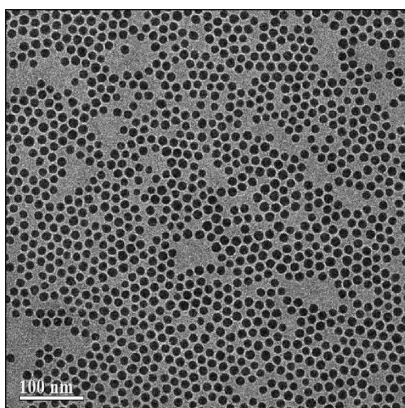


**Figure 5.** Nickel NPs synthesized with 4 OA and 4 TOP (15 nm,  $\sigma < 7.3\%$ ).

The representative XRD spectra obtained of the dried sample of the nanoparticles of monodispersed 9 nm, 32 nm, and polydispersed 50–80 nm (ESI) show a classic face-centered cubic unit cell for the Ni nanoparticles.

The TEM allows an access to the size of the particles. However, it does not provide readily information on the crystallinity and the size of the crystalline domains of the particles. The mean size of the crystallites was therefore evaluated using the Scherrer formula<sup>29</sup> (Table 1). The results are quite interesting, and representative examples are presented. Crystallite sizes are systematically much smaller than measured particle sizes by TEM, indicating that the nanoparticles are not single crystals. This is consistent with HRTEM and dark-field observations showing more than one crystallized domain in the nanoparticles (see ESI). Larger crystalline domains (entry 1) are obtained when only OA is used (both reducing agent and potential ligand), namely a poor ligand of Ni species. On the contrary, TOP strongly limits the growth of the monocrystals to about 5 nm, even with substoichiometric amounts.

(29) Scherrer formula for spherical particles

$$D = \frac{\lambda \kappa}{(B - B_0) \cos(\theta)}$$

with  $D$  being the mean diameter of the crystallites,  $\lambda = 1.54 \text{ \AA}$ ,  $\kappa = 0.89$ ,  $B_0 = 0.1^\circ$  (device correction), and  $B$  is the full width at half-maximum.  $B$  was evaluated using TOPAS software, with baseline correction and deconvolution.

When 4 equiv of TOP is used in the synthesis, the crystal lattices of the nanoparticles lose their long-range order, and only a broad correlation signal can be observed by XRD (see ESI). It is centered at  $44.7^\circ$ , which corresponds to a correlation distance of  $1.09 \text{ \AA}$ , in the range of Ni–Ni average distance in the solid state. A second broad signal, weaker, is also observed around  $77^\circ$ , very similar to the one at  $76.5^\circ$  from Ni fcc lattice. This confirms the formation of nearly amorphous Ni nanoparticles.<sup>31</sup> These observations pinpoint the role of a secondary aggregation process of crystalline small nanoparticles initially stabilized by TOP for the final size control of the particles: with the decrease of TOP amount, the surface stabilization becomes weaker and the growth of crystallized nuclei is favored.

**2.6. Growth Mechanisms.** The paramount influence of TOP stoichiometry on the size of the crystallized domains in the particles supports a growth mechanism involving aggregation of small nuclei. To confirm that point, a TEM study on the evolution of the nanoparticles size and morphology right after the start of the reaction was achieved by sampling and analyzing the reaction mixture at different times. The synthesis was then conducted using average conditions (2 equiv of TOP and 10 equiv of OA). Aliquots from the reaction mixture were readily cooled by dilution in hexanes. After 8 min of heating at  $220^\circ\text{C}$ , only small clusters of 2–3 nm practically spherical can be observed by TEM (Figure 6a). They remain well dispersed on the TEM grid, indicating that they are already protected by a shell of ligands.

After 15 min of heating, larger and polydispersed particles are observed (from 5 to 15 nm, Figure 6b, left). Their shapes (sometimes concave) suggest that they result from an aggregation of the small 2–3 nm nuclei. This is

- (30) This defocusing ripening cannot be definitely characterized as an Ostwald ripening (ripening with a constant concentration of monomers in solution), since the concentration of monomers in solution (here, Ni(0) molecular species) may still be decreasing.
- (31) Note that the temperature required for the decomposition of TOP is in the  $280$ – $350^\circ\text{C}$  range, giving  $\text{Ni}_2\text{P}$  as one of the resulting products. This phase has never been detected in this study. Even if J. B. Tracy et al. propose that this decomposition can start at  $240^\circ\text{C}$ , no decomposition of TOP at  $220^\circ\text{C}$  has ever been reported, to the best of our knowledge. See: Chen, Y.; She, H.; Luo, X.; Yue, G.-H.; Peng, D.-L. *J. Cryst. Growth* **2009**, *311*, 1229. Wang, J.; Johnston-Peck, A. C.; Tracy, J. B. *Chem. Mater.* **2009**, *21*, 4462.

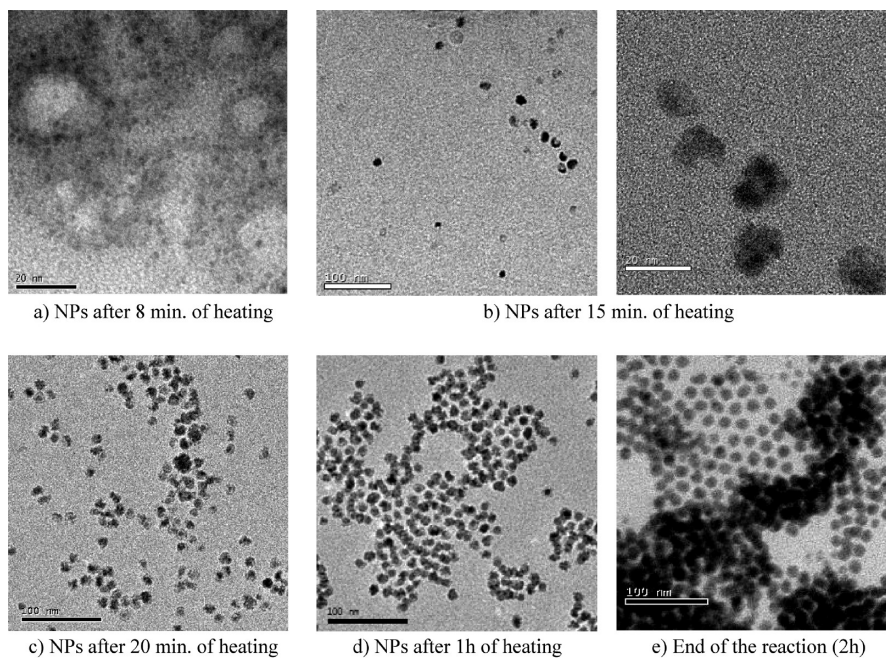


**Figure 6.** Qualitative TEM study on the growth mechanism of the nanoparticles.

confirmed by the presence of contrasted domain of this size within the same particle (Figure 6b, right).

After 20 min of heating (Figure 6c), the size dispersity is qualitatively much lower, most of the nanoparticles are in the range 11–15 nm, and practically no isolated nuclei could be observed. Most of the particles now show a convex morphology, which is energetically favored compared to the concave shape (due to smaller surface-to-volume ratio). After 20 min, the first-generation nuclei have then aggregated with other nuclei to give five-time bigger particles stabilized by a shell of ligands. After 1 h of heating (Figure 6d), the mean size is the same (12 nm) but the polydispersity is now very low, and the nanoparticles start to self-assemble in 2D hexagonal lattice onto the TEM grid, as observed on many samples presented before. The contrast observed within a particle is more homogeneous; however, the surface of the particles is still coarse. At the end of the reaction (2 h of heating, Figure 6e), the particles are spherical (14 nm), thus highlighting the beginning of ripening processes, but contrasted domains still appear in the particles.

This qualitative study demonstrates the existence of controlled aggregation processes in this synthesis and correlates well with the observation of multiple-crystallized domains inside the nanoparticles. Even in this highly simplified system (one temperature, one single metal precursor, one single reductant, and one main ligand), growth processes involve complex mechanisms: the nucleation rate still correlates with the supersaturation of the solution (so-called ‘LaMer mechanism’), but the following steps include a ligand-directed controlled aggregation of the nuclei, leading quickly to bigger but less crystallized nanoparticles.

**2.7. Ripening Mechanisms.** It was shown above that in some instances nanoparticles were faceted, whereas others remained spherical despite similar experimental conditions (reaction time, temperature). This suggested that ripening

processes (size evolution, shape evolution, or both) depending on the ligand (nature and quantity) could be occurring. In order to uncover these mechanisms, the influence of the reaction time was probed for various combinations of systems (OA and TOP). Representative experiments are presented below. First, in a mixture containing 0.8 equiv of TOP and 4 equiv of amine, no size defocusing effect was observed, but the particles became more faceted after 10 h of heating, displaying sharp edges (Figure 7, left-hand side). The nanoparticles therefore undergo only digestive ripening, which does not affect their size but promotes an intraparticulate reorganization of the nickel atoms.<sup>5</sup> On the other hand, when more than one equiv of TOP was used, a longer reaction time led to significant changes in the size and shape of the particles (Figure 7, right-hand side). For example, in a mixture containing 4 equiv of TOP and 4 equiv of OA, the standard deviation increased quickly with the duration of the experiment, from 7.3% after 2 h to 20.2% after 9 h. In this case, the nanoparticles undergo a defocusing ripening, the smaller dissolve and the larger grow, leading to a defocalization of their sizes.<sup>30</sup> This is corroborated by the observation of smaller particles at intermediate heating time (4 h) which have disappeared after 9 h. The particles remained nevertheless very spherical. The prominent role of low-concentrated Ni<sup>(0)</sup>-TOP mononuclear complexes, such as [Ni(TOP)<sub>4</sub>]<sup>2-</sup>, already identified in a similar system,<sup>25</sup> can be postulated. These species should act as Ni-atom soluble carriers, promoting the transfer of Ni between nanoparticles. The presence of large amounts of TOP favors formation of such mononuclear species which could then favor the transport of one nickel atom to another. Therefore, this can explain the shift from a digestive ripening process to a defocusing ripening upon increasing the phosphine amount.

**2.8. Surface State of the Nanoparticles.** Since many properties are influenced by the surface state of the nanoparticles, we next investigated the precise nature of

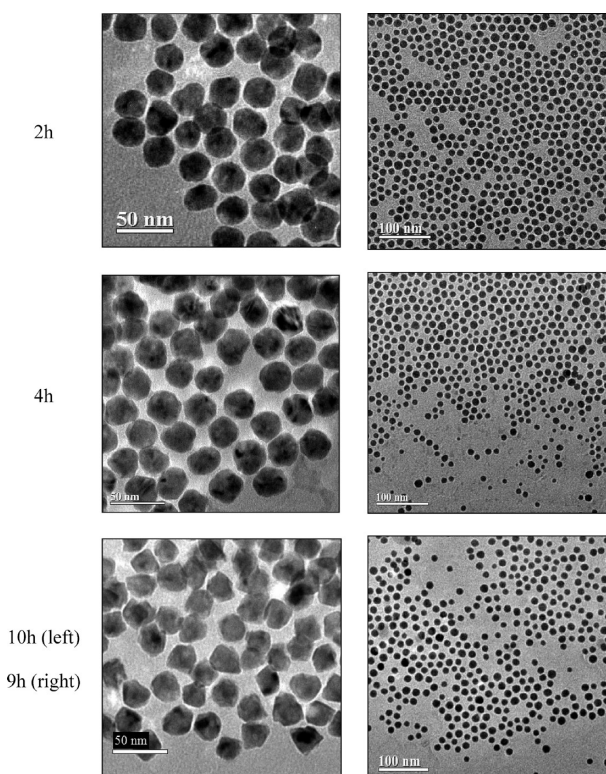


**Figure 7.** Left, ripening of the particles with 0.8 TOP and 4 OA and right, ripening of the particles with 4 TOP and 4 OA.

the particles organic coating. EDAX characterization of the nanoparticles shows the presence of phosphorus, which necessarily comes from the phosphine, near the inorganic core of the nanoparticles (see ESI). Indeed, the TEM grid are prepared after centrifugation of the nanoparticles and washing of excess ligands. Moreover, the P–C bond of TOP is not decomposed at the working temperature ( $220\text{ }^{\circ}\text{C}$ ).<sup>31</sup> The phosphorus observed by EDAX then attests for the presence of phosphine at the surface of the nanoparticles. Nitrogen compounds are not readily identified by this technique and in an attempt to characterize the surface ligands of the nanoparticles a posteriori, a sensitive technique for a system containing both organic and inorganic compounds was used: FTIR. Spectra of different samples were then recorded. Conclusions are presented here, and the complete set of spectra and analyses are found in the ESI.

In order to provide a reference, a nanoparticle synthesis with only OA was carried out. As mentioned above, it provides magnetic particles which readily agglomerate. The spectrum of isolated nanoparticles presents a very weak signal/ratio (spectrum P1 in the ESI), which clearly shows that only weak ligands, readily washed away, are bound on the surface in this case. However, new broad weak signals above  $1500\text{ cm}^{-1}$  are observed in the spectrum in addition to those of OA. They must belong to one (or several) byproduct(s) of the reduction of  $[\text{Ni}(\text{acac})_2]$  by OA. On the contrary, the FTIR spectrum of isolated nanoparticles synthesized with 2 equiv of TOP show the presence of two very broad signals at  $988$  and  $1051\text{ cm}^{-1}$  (see Figure 8 spectrum 1a and ESI), necessarily resulting from the coordination of the phosphine on the surface of

the particles, confirming the EDAX analysis. Yet, at this point, because pure TOP and OA have very similar IR signatures (Figure 8 spectra 4 and 5), the implication of OA as a second type of ligand on the particles cannot be ruled out, although it was shown above that this weak ligand is readily washed away. In order to finally discriminate between these two families of potential ligands, analogous experiments were carried out in the presence of  $\text{PPh}_3$  instead of TOP. Indeed,  $\text{PPh}_3$  and OA possess very different IR signatures (Figure 8 spectrum 6), thanks to the weak C–H stretching vibration above  $3000\text{ cm}^{-1}$  and the out-of-the-plane vibrations at  $742$  and  $692\text{ cm}^{-1}$ . As a ligand,  $\text{PPh}_3$  behaves in a similar manner as TOP in the synthesis of Ni nanoparticles.<sup>19</sup>

Like TOP,  $\text{PPh}_3$  is shown to be bound to the nanoparticles (Figure 8 spectrum 1 and ESI spectra 4 and 5), as shown by the appearance of signals at  $1063$  and  $960\text{ cm}^{-1}$ , attributed to aromatic C–H in-plane vibrations from coordinated  $\text{PPh}_3$ . The analysis of the supernatant shows the absence of  $\text{OPPh}_3$  before the first washing (spectra 2 and 7). Moreover, a second ligand containing an aliphatic chain (different from the oleylamine which is readily washed away) is found to remain near the surface of the particles after two washings (C–H stretching vibrations at  $2925$  and  $2852\text{ cm}^{-1}$ ). This organic product results probably from the reaction of OA with acac–Ni fragment and is relatively weakly bound to the surface (physisorption is proposed) since its vibration modes are not affected by the metal proximity. Also, an oxidation of the phosphine on the surface of the particles is found at air contact, because of the appearance of a vibration at  $1080\text{ cm}^{-1}$  after washing (proposed to be a Ni bound  $\text{P}=\text{O}$  stretching band, in accord with Brock et al.<sup>32</sup>). Since the spontaneous oxidation of  $\text{PPh}_3$  by  $\text{O}_2$ , either in the solid state or in solution, is very slow at air contact<sup>33</sup> (contrary to the oxidation of TOP), we propose that the nickel surface acts as a catalyst in this process. This point was investigated at last (ESI spectra 6 to 8) by an exchange of ligand using 1-butanethiol (Figure 8 spectrum 3). Indeed, thiol-covered nanoparticles do not exhibit the broad vibrations between  $950$  and  $1100\text{ cm}^{-1}$  resulting from phosphine and phosphine oxide coordination, confirming the paramount role of the nickel surface for the oxidation of the phosphine at air contact.

In this study, the implication of the phosphine as the main ligand was demonstrated, and the presence of other organic byproduct near the surface of the nanoparticles was evidenced. To reach a more complete description, we are currently studying the dynamic aspects of ligand exchange on the particles by solution-NMR techniques (pulsed gradient NMR or DOSY).

**2.9. SQUID.** In the perspective application of these designed monodispersed particles, magnetic measurement were realized on two samples of nanoparticles. The first sample analyzed was composed of 21 nm nanoparticles

(32) Senevirathne, K.; Burns, A. W.; Bussell, M. E.; Brock, S. L. *Adv. Funct. Mater.* **2007**, *17*, 3933.

(33) Commercial  $\text{PPh}_3$  is stable for years at the solid state in air condition. No spontaneous oxidation of  $\text{PPh}_3$  in solution in acetone was observed within 24 h.

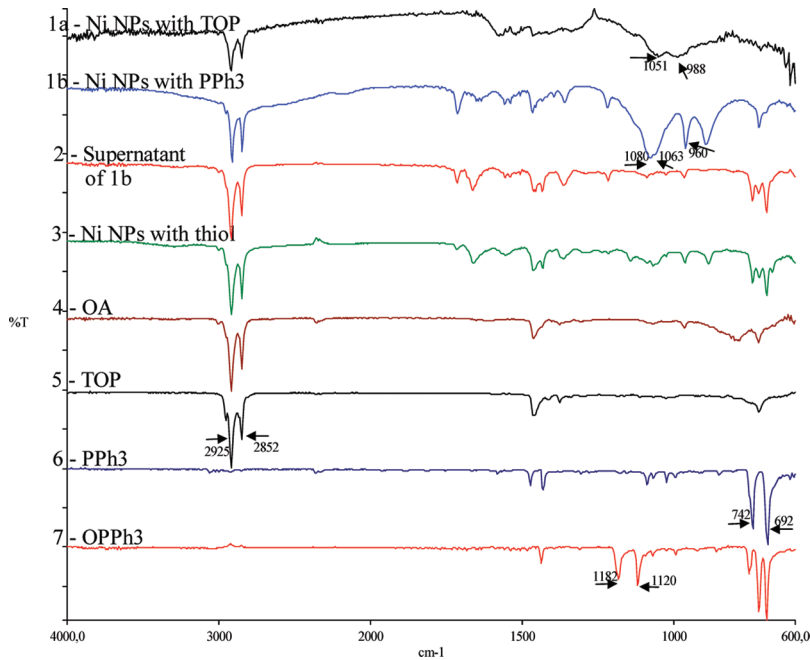


**Figure 8.** IR study of isolated nanoparticles (1a with TOP and 1b with PPh<sub>3</sub>), the supernatant of the reaction (2), after ligand exchange with 1-butanethiol (3), and reference spectra of the organic compounds (4–7).

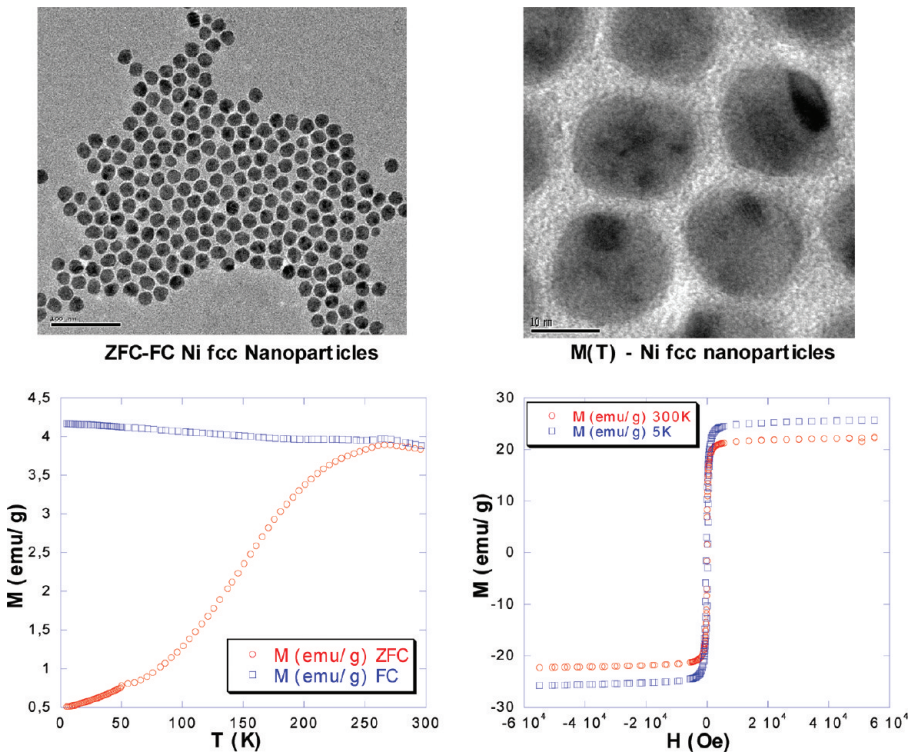


**Figure 9.** Sample A. TEM on the 21 nm fcc Ni nanoparticles (top); temperature-dependence on the magnetization M(T) (right) and variable field magnetization M(H) (left).

( $\sigma < 4.1\%$ ) with a Ni fcc structure. Nonreversibility of ZFC and FC plots indicates a superparamagnetic behavior with a temperature of superpara-paramagnetic transition at 270 K. The saturation magnetization is measured at 25 emu/g. The coercivity of 266 Oe is bigger than the coercivity of bulk nickel (0.7 Oe). A remanent magnetization of 10 emu/g is observed at 5 K. These results are comparable to the value obtained for bigger

fcc particles<sup>21</sup> and show a classical behavior for Ni nanoparticles.

We then turned our attention to less crystalline nanoparticles. SQUID measurements were made on a sample containing 12 nm Ni nanoparticles ( $\sigma \sim 10\%$ ) with a poor crystalline order (see section 2.5). The magnetic properties of these nanoparticles are quite different from the previous one (sample B, Figure 10, middle graphs). On

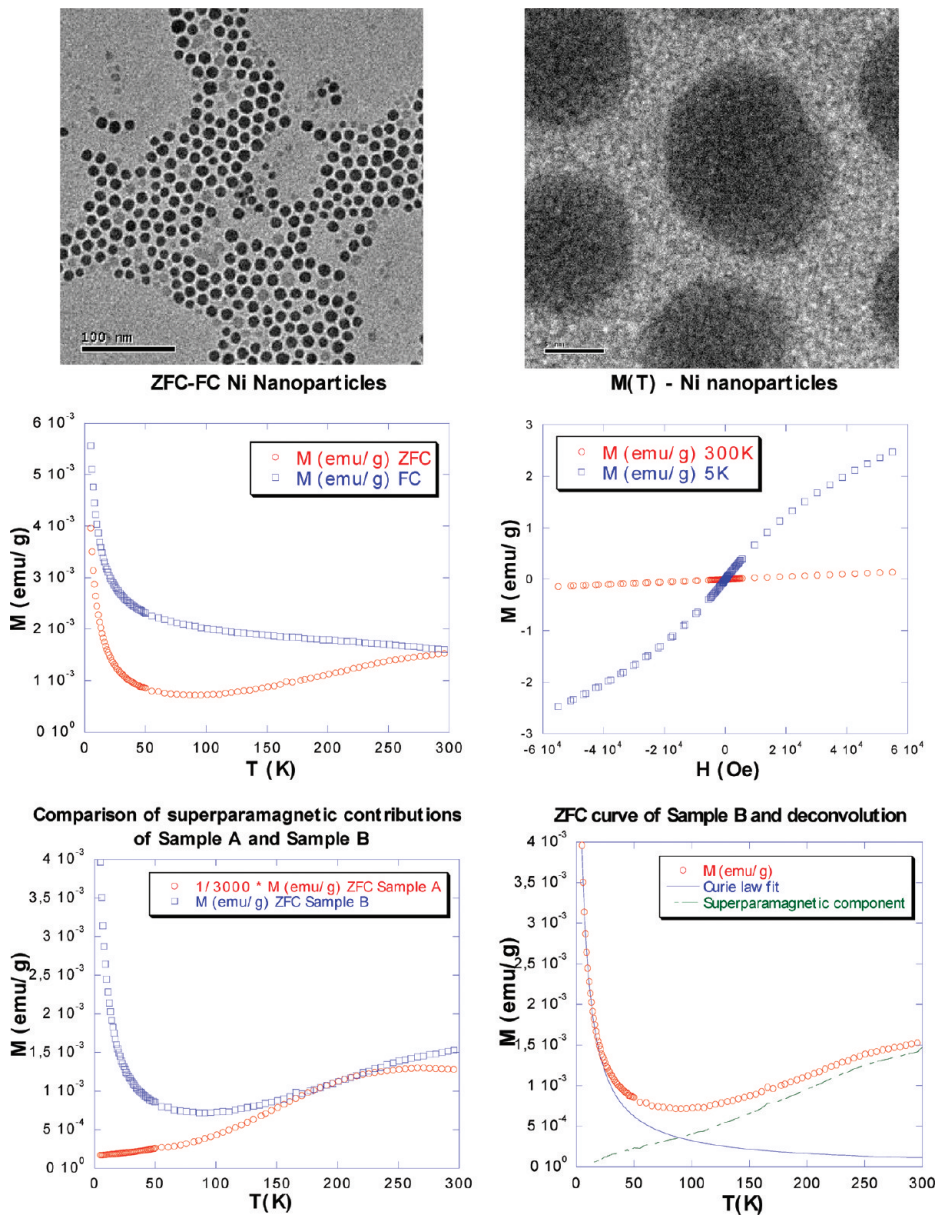


**Figure 10.** Sample B. Top: TEM on the 12 nm Ni nanoparticles. Middle: temperature-dependence on the magnetization  $M(T)$  (right) and variable field magnetization ( $M(H)$ ) (left). Bottom: ZFC curves comparison of sample A and sample B at 1/3000 scale (left) and deconvolution of the paramagnetic and superparamagnetic components (right).

the bottom-right graph of Figure 10, the ZFC curve of sample B is compared with the rescaled ZFC curve of sample A (scale 1/3000). The signal detected on sample B appears to be composed of a major fraction (> 99.9%) of a paramagnetic product with a Curie behavior, and a very small fraction of a superparamagnetic product very similar to the Ni fcc nanoparticles previously measured (but with a Curie temperature slightly above 300 K), even if this component could also come from a few ferromagnetic impurities (a deconvolution of these two contributions is proposed on Figure 10, bottom left). This preliminary characterization clearly points out that these poorly crystallized Ni nanoparticles display very different responses than fcc Ni nanoparticles and may find different applications in the field of magnetism. An extensive study of this phenomenon is currently underway in our laboratories.

In conclusion, the different factors which allow the synthesis of monodispersed, size tunable (ca. 2 to 30 nm) nickel particles by the thermal decomposition of a Ni(II) complex have been uncovered. Namely, the primary amine allows for a fast reduction of the precursor at 220 °C, and the phosphine allows for the precise size control. This control arises both from an efficient temperature-controlled nucleation step and a growth mechanism involving controlled aggregation, as evidenced by TEM study. In the course of our studies, two mechanisms of ripening of the Ni particles have been observed. The occurrence of either one or the other (or both) depends on the amount of phosphine ligand. The Ni particles prepared here possess a colloidal stability for weeks in alkane solvents, making them a relevant starting material for a thorough study of size-dependent properties or the development of new supported catalysts. In this

perspective, the precise composition of the shell of ligands for isolated nanoparticles was investigated. Ni nanoparticles stabilized by phosphine ligands are indeed good candidates for catalytic application in homogeneous<sup>19</sup> or heterogeneous systems.<sup>34</sup> They constitute also relevant nanobuilding blocks for the development of new nanomaterials. Preliminary SQUID measurements are presented in this purpose. Studies in this direction as well as to clarify the dynamic aspects of the nucleation and stabilization of the nickel nanoparticles are underway in our groups.

### 3. Experimental Section

All reactions were carried out under nitrogen atmosphere using standard air-free techniques.<sup>35</sup> Oleylamine (Aldrich, 70%) and trioctylphosphine (Strem, 97%) were used in the preparation described here without further purification.

**3.1. Synthesis of Nickel Nanoparticles in the Presence of TOP Alone.** Ni(acac)<sub>2</sub> (2.00 g, 7.80 mmol) was added to 78.0 mmol of trioctylphosphine (28.9 g, 10 equiv). The mixture was degassed at 100 °C and then heated at 220 °C for 2 h under inert atmosphere. The mixture was cooled to room temperature and centrifuged after addition of 40 mL of acetone to give a black product. The nanoparticles were redispersed in hexanes.

**3.2. Synthesis of Nickel Nanoparticles: Reduction by OA.** Ni(acac)<sub>2</sub> (2.00 g, 7.80 mmol) was added to 78.0 mmol of oleylamine (20.8 g, 10 equiv). The mixture was degassed at 100 °C and then heated at 220 °C for 2 h under inert atmosphere, giving quickly a black solution. The mixture was cooled to room temperature and centrifuged after addition of 40 mL of acetone to give a black product. The nanoparticles were redispersed in hexanes.

**3.3. Synthesis of Nickel Nanoparticles: Reduction by OA in the Presence of TOP.** Ni(acac)<sub>2</sub> (2.00 g, 7.80 mmol) was added to 78.0 mmol of oleylamine (20.8 g, 10 equiv) and 6.24 mmol of TOP (2.30 g, 0.8 equiv). The Ni/TOP and Ni/OA ratios were obtained by changing the amount of TOP or OA, and 1-octadecene was added if necessary in the other synthesis to keep the total volume of the mixture constant. The mixture was degassed at 100 °C and then heated at 220 °C for 2 h under inert atmosphere, giving quickly a black solution. The mixture was cooled to room temperature and centrifuged after addition of 40 mL of acetone to give a black product. The nanoparticles were redispersed in hexanes.

All the syntheses were carried out using a 100 mL trinecked flask and a heating mantle (C. Roth, WGH2R, 100 mL). The temperature was monitored from within the flask. Stirring was kept constant during the synthesis. The desired temperature was

set to the controller, resulting in a quick and reproducible heating (less than 10 min are necessary for the solution to reach the temperature of 220 °C). After heating, the mantle was immediately removed, and no other action was taken. The results of the syntheses were found to be also very sensitive to the heating device. A slight increase of the heating power results in a slight decrease of the size of the nanoparticles, due to a higher nucleation rate. The syntheses were all carried at a constant total volume to prevent the interference of any concentration or volume effects on the heating.

**3.4. Characterization.** Powder XRD measurements were performed with a Bruker D8 X-ray diffractometer operating in the reflection mode at Cu K $\alpha$  radiation with 40 kV beam voltage and 40 mA beam current. The data were collected in the 30–80° range (2 $\theta$ ) with steps of 0.05° and a counting time of at least 10 s.

**Transmission Electron Microscopy (TEM).** Samples were prepared by evaporating a drop of hexane diluted suspension of the nanoparticles on a carbon-coated copper grid. The nanoparticles were studied using a Philips CM12 (120 kV) and a Philips CM30 (300 kV) apparatus. The mean size and standard deviation were measured with the software DigitalMicrograph on at least 100 nanoparticles on two separated sites on the TEM grid.

**NMR spectra** were recorded on a Bruker AMX-300 spectrometer.

SQUID measurements were recorded using a Quantum Design MPMS 5 magnetometer. The measurements were recorded on very freshly synthesized nanoparticles kept under inert atmosphere as much as possible. ZFC and FC curves were recorded using a field of 50 Oe.

FTIR spectra were recorded using a Perkin-Elmer FTIR spectrometer Paragon 1000. A drop of the sample (liquid) or a few mg (solid) were deposited on the sample carrier without any treatment. The washing procedure consisted of adding 40 mL of acetone to the nanoparticles redispersed by ultrasound and centrifuging the suspension to recover a black solid.

**Acknowledgment.** The Laboratoire des Solides Irradiés (Ecole Polytechnique) is acknowledged for the use of their TEM. Pr. Anne Bleuzen and Dr. Eric Rivière from the Laboratoire de Chimie Inorganique (ICMO, Orsay) are gratefully acknowledged for the SQUID measurements and helpful discussion about the experimental results. S.C. thanks the DGA for financial support. The CNRS, the Ecole Polytechnique, and the UPMC are also thanked for financial support of this work.

**Supporting Information Available:** XRD-powder measurements, TEM and HRTEM observations of the nanoparticles, <sup>31</sup>P NMR spectra of the nanoparticles stabilized by TOP, EDAX analysis, and a complete set of spectra and detailed discussion concerning the FTIR study of the surface of the nanoparticles. This material is available free of charge via the Internet at <http://pubs.acs.org>.

(34) Lipshutz, B. H.; Tasler, S.; Chrisman, W.; Spliethoff, B.; Tesche, B. *J. Org. Chem.* **2003**, *68*, 1177.

(35) Shriver, D. F. *The Manipulation of Air-Sensitive Compounds*, 2nd ed.; Wiley Interscience: New York, 1986.